Available online at www.sciencedirect.com
ScienceDirect
International Journal of Heat and Mass Transfer 50 (2007) 1694–1705
International Journal of HEAT and MASS TRANSFER
www.elsevier.com/locate/ijhmt

One-dimensional ice growth due to incoming supercooled droplets impacting on a thin conducting substrate

T.W. Brakel, J.P.F. Charpin, T.G. Myers *

Department of Mathematics and Applied Mathematics, University of Cape Town, Rondebosch 7701, South Africa

Received 28 May 2005
Available online 8 December 2006

Abstract

A one-dimensional model for ice accretion due to incoming supercooled water impacting on a conducting substrate is developed, where the substrate is cooled from below by a liquid or gas. Both rime and glaze ice situations are considered. Non-dimensionalisation shows that conduction is the dominant method of heat transfer and so the heat equations are reduced to pseudo-steady forms. In this case the problem reduces to solving a single equation for the ice layer thickness. The water height and temperatures in the ice, water and substrate may subsequently be found. The asymptotic solution is validated by comparison with results from a numerical scheme which solves the full Stefan problem. This is an extension of a previously published solution method that involved simpler boundary conditions. For glaze ice, a comparison including water droplet energy either in the boundary conditions or as a source term in the heat equations, is also performed.

1. Introduction

Ice accretion on structures, aircraft, ships and refrigeration equipment is a problem that has plagued engineers for many years [1,2]. Consequently there are numerous, complex models for the icing process. These typically involve modelling the surrounding air flow field, water droplet trajectories and then the actual accretion process. All three components are coupled. However, the key to all icing models is implementing the correct basic energy balance. It is this balance that forms the backbone of all current icing models and this is the subject of the current paper.

The seminal work on ice accretion was carried out by Stefan in the 1800s, see [3] for a comprehensive review of ice accretion modelling. In the aircraft industry possibly the most important work of this nature is the one-dimensional equilibrium energy balance of Messinger [4]. This model describes the basic balance employed in most current commercial icing models (not just in the aircraft industry). However, it has a number of drawbacks and in fact will always lead to a slower rate of ice accretion than occurs in practice [5]. The error will increase as the ambient temperature increases and hence it is at its worst in mild conditions. Unfortunately it is in mild conditions that ice accretion is most unpredictable. In this case there is often a significant water layer on top of the ice which may flow and consequently lead to ice appearing away from an impingement zone. Gent et al. [1] point out that icing models can now only progress significantly if the Messinger based models are replaced by more realistic ones.

In a series of papers Myers and co-workers have developed models for ice accretion with water flow due to supercooled water impacting on a cold surface [5–8]. The models have been tested against experimental results and are currently employed in a commercial three-dimensional aircraft icing code, ICECREMO, see [1,9] for example. Initially the work deals with the one-dimensional model, attempting to remove the deficiencies of the Messinger model [5,6]. This one-dimensional model has subsequently been used

* Corresponding author. Present address: Division of Applied Mathematics, KAIST 373-1 Guseong-dong, Yuseong-gu, Daejeon 305-701, Republic of Korea. Tel.: +27 21 6503815; fax: +27 21 6502334.
E-mail address: myers@maths.uct.ac.za (T.G. Myers).

0017-9310/$ - see front matter © 2006 Elsevier Ltd. All rights reserved.
doi:10.1016/j.ijheatmasstransfer.2006.10.014

Nomenclature

b	ice layer thickness
c	specific heat capacity
$e(T) \approx e_0 T$	saturation vapour pressure
H	convective heat transfer coefficient
h	water layer thickness
k	thermal conductivity
L	substrate height
L_f	latent heat of freezing
$\dot{m}$	incoming water mass flux (normalised by area)
q	sum of energy source or sink terms
Q	energy source or sink terms
r	local recovery factor
S	Stefan number
t	time variable
T	temperature in ice
$T_{\text{subscript}}$	constant temperature for region denoted with subscript below
w	free stream air velocity
x	spatial variable
β	local collection efficiency
ρ	density
θ	temperature in water layer
χ	temperature in substrate
λ_e	evaporation coefficient
λ_s	sublimation coefficient

Subscripts

a	air above ice or water layer
A	air beneath substrate
i	ice layer or grid point index in numerical solution
k	temporal index in numerical solution
s	substrate
w	water

extensively in a series of papers by Naterer, see [10] and references therein, in a study of structural icing. In [7] the work is advanced to couple the one-dimensional model to a water flow component. In Myers et al. [8] a model for combined water flow and accretion on an arbitrary shaped substrate is described, the application to practical situations is detailed in [11].

As mentioned, this hierarchy of models was constructed as part of a program to develop a commercial code. Due to the time constraints and the specific nature of the investigation a number of questions and extensions related to the one-dimensional model were not investigated. These will be considered in the current paper.

Firstly, in the one-dimensional model of [5,6] heat equations were defined in the ice and water layers, subject to either a fixed temperature substrate or a cooling condition. The equations and boundary conditions were non-dimensionalised to highlight the dominant terms. This demonstrated that the time derivatives in the two heat equations were negligible. Taking the coefficients of the time derivatives as small parameters an asymptotic expansion then led to a leading order problem which was pseudo-steady, *i.e.* time enters only through the boundary conditions, see [12] for other examples where pseudo-steady models are employed. Physically this means that the ice accretion rate is significantly slower than the heat conduction rate. In general asymptotic approximations can provide excellent solutions, however there may be problems in applying appropriate boundary, or in this case initial conditions. When conditions cannot be applied it is termed a singular perturbation, see [13] for example. In the model of [5,6] neglecting the time-derivative in the leading order equation meant that the initial condition could not be applied. The effect of this was never investigated. In the following we will use a similar asymptotic expansion but will also compare it with a full numerical scheme to validate solutions for all times.

Secondly, since the model was part of the initial phase of the aircraft icing program, anti- and de-icing techniques were not considered. However, Gent et al. [1] point out that understanding ice formation is only a pre-requisite to understanding its removal and thus developing an anti or de-icing system. The ability to model heat flow through the substrate is therefore an essential step in this process. To do this we must extend the previous model to deal with heat flow in three regions, namely ice, water and substrate, and these are coupled at two boundaries. This will make the model significantly more complex than that described in [6,7]. However, it will not only provide a basis for modelling certain types of ice protection systems, but will also permit the prediction of ice formation above cold spots. Cold spots occur, for example, when an aircraft flies through a cold region causing the fuel to cool down. When the plane flies into a warmer region anti-icing may no longer seem appropriate but the cold fuel may extract warmth from the surface and cool it below freezing.

Finally, when glaze ice is forming, there is a layer of water on top of the ice. The layer is cooled at its top surface by the free stream air flow and it is constantly fed by incoming water droplets. In the original model all the energy source and sink terms experienced by the water were applied at the top surface. In reality some of the energy terms should be applied within the film. For example the water droplets are at a different temperature to the film. When they impact they will pierce the film and mix with it. Their energy will thus be imparted throughout the film, not just at the surface. Similarly with their kinetic energy. Naterer [10] states that the droplet kinetic energy will be distributed throughout the film as the droplets pass through. However, he was unable to incorporate the

appropriate modification into the model and so adapted the model of [6,7] to include the kinetic energy in the Stefan condition, *i.e.* all of the droplet kinetic energy is imparted at the ice interface. The droplet temperature (or sensible heat) was still applied at the air–water boundary.

It is possible that, since the film is thin, applying all of the energy terms at the boundary is a reasonable approximation. Effectively this means we are linearising the boundary condition, based on the thinness of the region. However, the validity of this approach has not been investigated. Naterer [10] mentions carrying out a sensitivity study which shows that adding kinetic energy to the Stefan condition does not greatly affect the ice growth rate. However, it is not stated under what conditions this study was carried out and obviously the conclusion does not apply to adding both the droplet heat and kinetic energy within the film. A study of this issue will be carried out in Sections 3.2.1 and 3.2.2.

In the following Section 2, we will describe the mathematical model. Non-dimensionalisation will then be used to identify small parameters and therefore how to proceed with the asymptotic expansion. The leading order solution will be examined in Section 3. The full numerical solution will then be described in Section 4. In Section 5 the asymptotic results will be compared with the numerics, under conditions appropriate to structural and aircraft icing, to verify the accuracy of the asymptotic solutions.

2. One-dimensional thermal analysis

Consider a situation where supercooled water droplets impact on a thin conducting surface at a rate $\dot{m}$. If the surface is below the freezing temperature the droplets will freeze almost instantaneously to form a rime ice layer. In mild temperatures or in the presence of a sufficiently thick ice layer, a water layer may subsequently appear and glaze ice will then form. This is depicted in Fig. 1. The temperatures in the substrate, ice and water are denoted with $\chi(x,t)$, $T(x,t)$, $\theta(x,t)$ respectively, and the thicknesses of the three layers are L, $b(t)$, $h(t)$. In the following analysis we will assume that when glaze ice forms all of the energy from the droplets is transmitted to the film at the free surface. In Section 3.2.2 we will modify this to distribute the energy through the film.

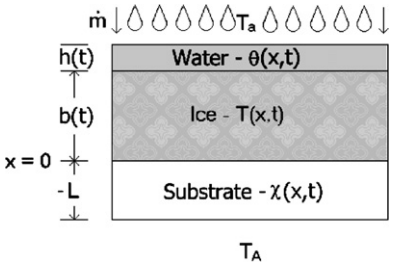

Fig. 1. Schematic of model problem.

In order to describe this situation mathematically heat equations must be specified for each layer:

$$\rho_s c_s \frac{\partial \chi}{\partial t} = k_s \frac{\partial^2 \chi}{\partial x^2}, \quad -L \leqslant x \leqslant 0, \tag{1}$$

$$\rho_i c_i \frac{\partial T}{\partial t} = k_i \frac{\partial^2 T}{\partial x^2}, \quad 0 \leqslant x \leqslant b, \tag{2}$$

$$\rho_w c_w \frac{\partial \theta}{\partial t} = k_w \frac{\partial^2 \theta}{\partial x^2}, \quad b \leqslant x \leqslant b + h. \tag{3}$$

Eqs. (1)–(3) are solved subject to the following boundary conditions. Underneath the substrate there is cooling due to the flow of air at temperature T_A:

$$k_s \frac{\partial \chi}{\partial x} = H_{as}(\chi - T_A), \tag{4}$$

where H_{as} is the heat transfer coefficient at this interface. At the substrate/ice interface, $x = 0$, heat flux is conserved:

$$k_s \frac{\partial \chi}{\partial x} = H_{si}(T - \chi), \quad k_i \frac{\partial T}{\partial x} = H_{si}(T - \chi) \tag{5}$$

where H_{si} is the heat transfer coefficient between the ice and substrate.

Under rime ice conditions there is no water layer. At the top of the rime ice layer, heat energy is gained due to: kinetic energy, aerodynamic heating and the latent heat of freezing of the solidifying droplets. These are independent of the relative temperature between the ice and droplets, their sum is represented by Q_i, where

$$Q_i = \frac{1}{2}\dot{m}w^2 + \frac{rH_{ai}w^2}{2c_a} + \dot{m}L_f,$$

where $\dot{m}$ is the incoming mass flux per unit area of water, w is the far field air velocity, r is the local recovery factor, c_a is the heat capacity of air, H_{ai} is the heat transfer coefficient between ice and air. Energy is lost to the surrounding air (at temperature T_a) due to convective heat transfer and sublimation, since the droplets are cooler than the ice, energy is also lost in heating them up to the ice surface temperature

$$Q_l = (\dot{m}c_w + \lambda_s e_0 + H_{ai})(T_a - T) = q_l(T_a - T).$$

An energy balance then gives the boundary condition at the top of the ice layer, $x = b$:

$$k_i \frac{\partial T}{\partial x} = Q_i + q_l(T_a - T). \tag{6}$$

If glaze ice is growing, Eq. (3) must also be solved, with the following boundary conditions. At the ice/water interface, $x = b$, the temperature will remain constant at the melting temperature of ice T_f:

$$T = \theta = T_f. \tag{7}$$

At the top of the water layer, energy is gained due to kinetic energy and aerodynamic heating only:

$$Q_w = \frac{1}{2}\dot{m}w^2 + \frac{rH_{aw}w^2}{2c_a}. \tag{8}$$

Energy is lost due to convective heat transfer, evaporation and the thermal energy of the droplets:

$$Q_m = (\dot{m}c_w + \lambda_e e_0 + H_{aw})(T_a - \theta) = q_m(T_a - \theta).$$

The boundary condition at the top of the water layer $x = b + h$ may therefore be written:

$$k_w \frac{\partial \theta}{\partial x} = Q_w + q_m(T_a - \theta). \tag{9}$$

In the model studied in Section 3.2.2 the kinetic and thermal energy terms will be removed from Q_w and Q_m and taken as source terms in the water heat equation.

The system (1)–(3) involves three unknown temperatures and the two unknown thicknesses b and h. Closing the system requires two more equations. The first is a mass balance:

$$\rho_i \frac{\partial b}{\partial t} + \rho_w \frac{\partial h}{\partial t} = \dot{m}. \tag{10}$$

When rime ice forms h should be set to zero in the above equation and the system is closed subject to $b(0) = 0$. If glaze ice forms then an energy balance, the standard Stefan condition, must also be specified:

$$\rho_i L_f \frac{\partial b}{\partial t} = k_i \frac{\partial T}{\partial x} - k_w \frac{\partial \theta}{\partial x}. \tag{11}$$

This states that the energy required to make ice is the difference between the energy conducted away through the water and ice layers.

We now proceed to non-dimensionalise the system in order to define the dominant terms and therefore to simplify the governing equations. The length scale chosen is the width of the substrate. The time scale is proportional to the water deposition rate $\dot{m}$, since this dictates the growth rate of the ice layer. The temperature is scaled so T_a corresponds to 0, and T_f corresponds to 1. The following substitutions are therefore made to non-dimensionalise the system:

$$\hat{x} = \frac{x}{L}, \quad \hat{t} = \left(\frac{\dot{m}}{\rho_i L}\right)t, \quad (\hat{\chi}, \hat{T}, \hat{\theta}) = \frac{(\chi, T, \theta) - T_a}{\Delta T}, \tag{12}$$

where $\Delta T = T_f - T_a$ and hats denote non-dimensional quantities. For ease of notation we immediately drop the hats. These substitutions give the following forms for the heat equations:

$$\frac{\partial^2 \chi}{\partial x^2} = \epsilon_s \frac{\partial \chi}{\partial t}, \quad -1 \leqslant x \leqslant 0, \tag{13}$$

$$\frac{\partial^2 T}{\partial x^2} = \epsilon_i \frac{\partial T}{\partial t}, \quad 0 \leqslant x \leqslant b, \tag{14}$$

$$\frac{\partial^2 \theta}{\partial x^2} = \epsilon_w \frac{\partial \theta}{\partial t}, \quad b \leqslant x \leqslant b + h, \tag{15}$$

where

$$\epsilon_s = \frac{\rho_s c_s \dot{m} L}{\rho_i k_s}, \quad \epsilon_i = \frac{c_i L \dot{m}}{k_i}, \quad \epsilon_w = \frac{\rho_w c_w \dot{m} L}{\rho_i k_w}. \tag{16}$$

The mass and energy balances become

$$\frac{\partial b}{\partial t} + \frac{\rho_w}{\rho_i}\frac{\partial h}{\partial t} = 1, \tag{17}$$

$$S\frac{\partial b}{\partial t} = \frac{\partial T}{\partial x} - \frac{k_w}{k_i}\frac{\partial \theta}{\partial x}, \tag{18}$$

where the Stefan number $S = \dot{m}L_f L/k_i \Delta T$ and Eq. (18) is evaluated at the interface $x = b$.

Boundary conditions (4)–(9) reduce to

$$\chi_x = c_1 \chi|_{x=-1} + c_2, \quad \chi_x = c_3(T - \chi)|_{x=0}, \tag{19}$$

$$T_x = c_4(T - \chi)|_{x=0}, \quad T_x = c_5 - c_6 T|_{x=b}, \tag{20}$$

$$T(b,t) = \theta(b,t) = 1, \quad \theta_x = c_7 - c_8\theta|_{x=b+h}, \tag{21}$$

where

$$c_1 = \frac{H_{as}L}{k_s}, \quad c_2 = \frac{H_{as}L}{k_s}\frac{T_a - T_A}{\Delta T}, \quad c_3 = \frac{H_{si}L}{k_s}, \quad c_4 = \frac{H_{si}L}{k_i},$$
$$c_5 = \frac{Q_i L}{k_i \Delta T}, \quad c_6 = \frac{q_l L}{k_i}, \quad c_7 = \frac{Q_w L}{k_w \Delta T}, \quad c_8 = \frac{q_m L}{k_w}.$$

Material properties for the substrate, ice and water are presented in Table 1. The properties for the substrate material are those for a common aluminium alloy. Physical parameters typical for aircraft and structural icing are presented in Table 2. Under these conditions, $\epsilon_s = 0.001$,

Table 1
Properties of aluminium alloy, ice and water

c_s	1250	J/kg K
k_s	175	W/m K
ρ_s	2710	kg/m^3
T_f	273	K
c_i	2050	J/kg K
k_i	2.18	W/m K
ρ_i	917	kg/m^3
L_f	3.34×10^5	J/kg
c_w	4218	J/kg K
k_w	0.57	W/m K
ρ_w	1000	kg/m^3
c_a	1014	J/kg K

Table 2
Physical parameters for structural and aircraft icing conditions

Structural					
L	0.01	m	$\dot{m}$	0.005	kg/m^2 s
H_{ai}	500	W/m^2 K	H_{aw}	500	W/m^2 K
H_{as}	500	W/m^2 K	H_{si}	1000	W/m^2 K
w	5	m/s	r	0.5	
λ_s	9.3	m/s	λ_e	8.2	m/s
e_0	27.03	Pa/K			
Aircraft					
L	0.001	m	$\dot{m}$	0.05	kg/m^2 s
T_A	260	K	T_a	260	K
H_{ai}	500	W/m^2 K	H_{aw}	500	W/m^2 K
H_{as}	2000	W/m^2 K	H_{si}	1000	W/m^2 K
w	90	m/s	r	0.895	
λ_s	10.3	m/s	λ_e	9.1	m/s
e_0	27.03	Pa/K			

$\epsilon_i = 0.047$ and $\epsilon_w = 0.403$, $S = 3$. Further information on quantities such as the heat transfer coefficient and incoming mass rate can be found in [8].

Since $\epsilon_s, \epsilon_i \ll 1$ the time derivatives in (1) and (2) are, in general, negligible. ϵ_w is relatively large, however, it will be shown later that a sufficiently thin water layer forms for the time derivative in (3) to also be neglected. This is the same approach that was employed in [6,7]. In general the results will be accurate to within $\mathcal{O}(\epsilon)$, except for in the very initial stages, $t \sim \epsilon$, when the time derivative may in fact be the dominant term. In the case of ϵ_w the results will be significantly more accurate than $\mathcal{O}(\epsilon_w)$, except possibly during the initial stages. In the following section we will consider the asymptotic solution where each ϵ is treated as a small parameter. We will then move onto a numerical solution of the full equations to determine the validity of the approximate solution.

In the following work our primary interest is in thin substrates, such as the shell of an aircraft, or in situations where the heating elements are placed close to the surface and this motivates our choice of scaling, which in turn determines the values of ϵ. However, the analysis may be valid for much thicker substrates depending on the material parameters. For example, if the substrate is concrete then $\epsilon_s \ll 1$ requires $L \ll 10$ cm and we can work with substrates of the order of centimetres thick. However, in this case, $\epsilon_w \sim 1$ and it appears that the approximation is invalid in the water layer. The problem could be remedied by choosing a different length-scale in the ice and water layers, which in turn requires a different time-scale. To avoid this confusion we stick with a single scaling throughout the three layers and so restrict the analysis to relatively thin layers.

3. Asymptotic solutions

3.1. Rime ice growth

Rime ice growth is the simplest case. The ice thickness is determined by integrating Eq. (17) with $h \equiv 0$, so $b = t$. Since $\epsilon_i \gg \epsilon_s$ (in fact $\epsilon_s \sim \epsilon_i^2$), the temperature profiles take the form

$$\chi = \chi_0 + \epsilon_i \chi_1, \quad T = T_0 + \epsilon_i T_1.$$

The leading order heat equations are then

$$\frac{\partial^2 \chi_0}{\partial x^2} = 0, \quad \frac{\partial^2 T_0}{\partial x^2} = 0. \tag{22}$$

These must be solved subject to the leading order boundary conditions:

$$\frac{\partial \chi_0}{\partial x} = c_1 \chi_0 + c_2|_{x=-1}, \tag{23}$$

$$\frac{\partial \chi_0}{\partial x} = c_3 (T_0 - \chi_0)|_{x=0}, \quad \frac{\partial T_0}{\partial x} = c_4 (T_0 - \chi_0)|_{x=0}, \tag{24}$$

$$\frac{\partial T_0}{\partial x} = c_5 - c_6 T_0|_{x=b}. \tag{25}$$

At this stage the problem is clearly defined. The analytical solution is simple although cumbersome and can easily be dealt with by a standard computer algebra package such as MAPLE.

The leading order temperature profiles are therefore

$$\chi_0 = a_0 + a_1 x, \quad T_0 = a_2 + a_3 x, \tag{26}$$

where

$$a_0 = \frac{c_3 c_5 (1 + c_1) - c_2 c_4 (1 + b c_6) - c_2 c_6}{c_6 (c_1 + c_3 + c_1 c_3 + b c_1 c_4) + c_1 c_4},$$

$$a_1 = \frac{c_3}{c_4} a_3,$$

$$a_2 = \frac{c_5 (c_1 + c_3 + c_1 c_3) - c_2 c_4 (1 + b c_6)}{c_6 (c_1 + c_3 + c_1 c_3 + b c_1 c_4) + c_1 c_4},$$

$$a_3 = \frac{c_4 (c_1 c_5 + c_2 c_6)}{c_6 (c_1 + c_3 + c_1 c_3 + b c_1 c_4) + c_1 c_4}.$$

Eqs. (26) are clearly linear in x but, due to the presence of the moving boundary position, $b(t)$, they are non-linear in time.

The rime ice problem is now solved (at leading order). The temperature profiles in the substrate and ice layers are given by (26). The ice thickness is simply $b = t$. These equations remain valid until water first appears (if it does appear). This will occur when the ice surface, $x = b$, reaches the melting temperature $T(b) = 1$. To determine the thickness and hence the time at which this occurs we substitute $T = 1$ and $x = b_w$ into (26). Rearranging the expression leads to

$$b_w = \frac{c_4 (c_2 + c_1) - (c_1 c_3 + c_1 + c_3)(c_5 - c_6)}{c_4 c_1 (c_5 - c_6)}. \tag{27}$$

In fact there are three possible scenarios that (27) tells us about. In sufficiently cold conditions water will never appear, in this case Eq. (27) predicts a negative value for b_w. As conditions become milder water will appear at ice thickness $b_w > 0$. The transition between these two states is manifested by $b_w \to \pm\infty$, *i.e.* when $c_5 = c_6$. In terms of the physical variables this means when

$$T_a = T_f - \frac{Q_i}{q_l}. \tag{28}$$

Since Q_i represents the energy gain terms and q_l represents the energy loss terms this equation indicates that the ambient temperature at which water never appears decreases with increasing energy terms, such as faster droplet impact. If the energy loss terms increase, for example the incoming droplets become colder, then T_a increases. Finally, water will appear immediately when $b_w = 0$ (within the level of approximation used).

If $b_w = t_w \geqslant 0$ then a layer of water will appear at this time, subsequently the glaze ice model must be employed.

The form of b_w is shown in Fig. 2 for the situation where $T_A = T_a$. The two plots show results for aircraft and structural icing conditions. The values used are those given in

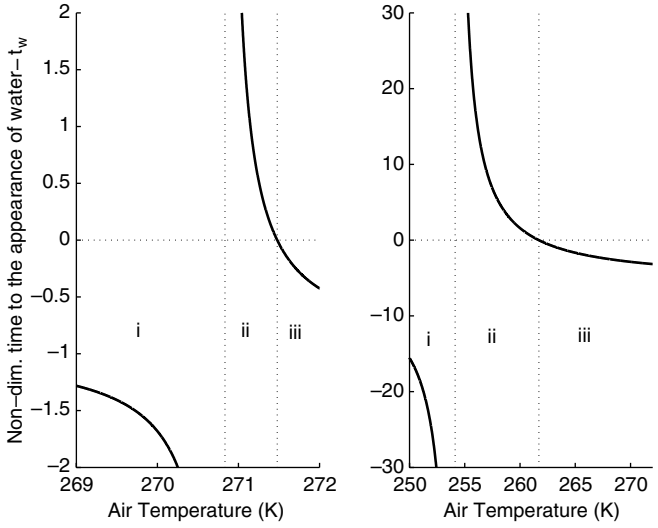

Fig. 2. Time to appearance of water when $T_a = T_A$ for (left) structural icing and (right) aircraft icing conditions.

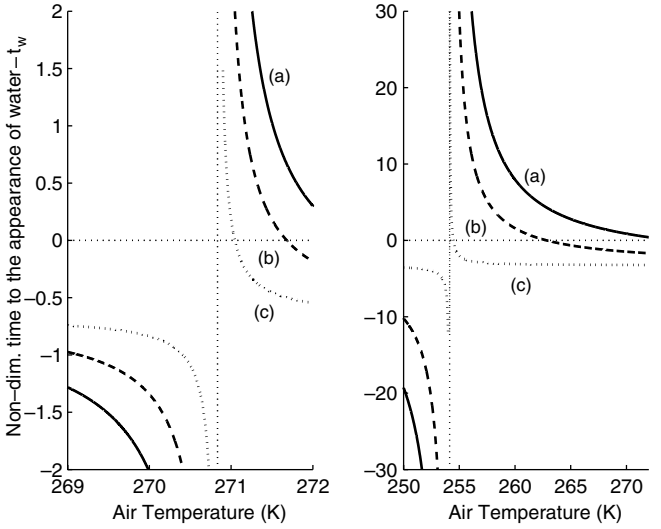

Fig. 3. Time to appearance of water for (left) structural icing: (a) 269, (b) 271, (c) 272.5 K and (right) aircraft icing: (a) 243, (b) 260, (c) 272.5 K conditions.

Table 2. The x-axis has been dimensionalised so the reader can relate the air temperature to actual physical conditions. The main difference is that glaze ice appears at lower temperatures and over a wider temperature range under aircraft conditions than structural icing.

Corresponding to the three scenarios discussed, three regions appear in Fig. 2, they have been enumerated from i to iii. Region i is where the air temperature is too cold for water to ever appear, in this case when $T_a < 270.8$ K for structural icing and $T_a < 254$ K for aircraft icing. As the air temperature increases we move into region ii. Here, water will appear after time $t_w = b_w$, indicating rime ice will be present initially; and a water layer will appear after time t_w. Region iii occurs when conditions are warmer and the theoretical time for water to appear is negative. This indicates that the model assumption, that ice will always be present, is incorrect and in this case water will appear first with no ice.

The models described in [6–11] deal with a substrate with a high thermal mass and hence employ a fixed temperature condition at the substrate, $T = T_s$ at $x = 0$. Substituting this for condition (24) and solving for the temperature we find the appropriate expression for b_w as $b_w = (1 - T_s)/(c_5 - c_6)$. So, surprisingly the condition for the transition from water appearing to no water is unaffected by the different condition, *i.e.* in both cases the transition is determined by (28). This means that to some extent the transition is unaffected by the substrate temperature. However, this temperature does enter into the numerator of the b_w expression. For water to appear at some stage the numerator must be positive. With the fixed substrate temperature we require $T_s < 1$ (or in dimensional form $T_s < T_f$). This means that ice can only appear if the substrate is below the freezing temperature. In the present case the situation is more complex, requiring the numerator of (27) to be positive.

In Fig. 3 we show results for different values of the temperature below the substrate, T_A. Of particular interest are the curves for the aircraft icing scenario. There we see that with $T_A = 243$ K, glaze ice can occur for external temperatures greater than 270 K. In fact by decreasing T_A we can predict ice for $T_a > T_f$. This is precisely the situation where ice forms above cold spots. When the temperature is relatively high, $T_A = 272.5$, ice will not occur unless the air temperature is below 254.5 K. Similar qualitative results are observed for the cable icing, but the variation occurs over a much narrower temperature range.

3.2. Glaze ice growth

3.2.1. Droplet energy in boundary condition

If b_w is positive (occurring in region ii of Fig. 2) the rime ice model is no longer valid for $b \geqslant b_w$ ($t \geqslant t_w$). In this case the temperature profile in all three layers must be determined. Neglecting all terms of $\mathcal{O}(\epsilon)$, the leading order solution to Eqs. (13)–(15) are

$$\chi_0 = d_0 + d_1 x, \quad T_0 = d_2 + d_3 x, \quad \theta_0 = d_4 + d_5 x. \tag{29}$$

Applying boundary conditions (19)–(21) leads to the following coefficients:

$$d_0 = \frac{c_1c_3 + c_3 - c_2 - c_4c_2b}{c_1c_3 + c_1 + c_1c_4b + c_3}, \quad d_1 = \frac{c_3(c_1 + c_2)}{c_1c_3 + c_1 + c_1c_4b + c_3},$$
$$d_2 = \frac{c_1 + c_1c_3 + c_3 - c_4c_2b}{c_1c_3 + c_1 + c_1c_4b + c_3},$$
$$d_3 = \frac{c_4}{c_3}d_1 = \frac{c_4(c_1 + c_2)}{c_1c_3 + c_1 + c_1c_4b + c_3},$$
$$d_4 = \frac{1 - bc_7 + c_8(b + h)}{1 + c_8h}, \quad d_5 = \frac{c_7 - c_8}{1 + c_8h}.$$

The coefficients d_i involve both the ice and water heights, b, h, and are therefore non-linear in time. The temperature profiles therefore require b and h to be determined. The water height may be expressed as a function of the ice height by integrating the mass conservation equation (17) with respect to t. Applying $h(t_w) = 0$ and $b(t_w) = t_w$ the water height may be written

$$h = \frac{\rho_i}{\rho_w}(t - b), \quad t \geqslant t_w. \tag{30}$$

This leaves the ice layer height b as the remaining unknown. The rate of change of the ice layer height will be governed by the temperature gradients at the ice/water interface and the latent heat released, specified by the Stefan condition. In non-dimensional form, the Stefan condition is (at $x = b$)

$$S\frac{\partial b}{\partial t} = d_3 - \frac{k_w}{k_i}d_5. \tag{31}$$

The water height may be eliminated from the expressions for d_3 and d_5 using (30). This leaves a non-linear equation for b as a function of t as the only equation to be solved:

$$\frac{\partial b}{\partial t} = S^{-1}\left(\frac{c_4(c_1 + c_2)}{c_1c_3 + c_1 + c_1c_4b + c_3} - \frac{k_w}{k_i}\frac{(c_7 - c_8)}{(1 + c_8\frac{\rho_i}{\rho_w}(t - b))}\right). \tag{32}$$

The numerical solution of this equation determines the ice thickness which in turn may be used to determine the water heights and then temperatures via (30) and (29).

3.2.2. Droplet energy as a source term

The above calculation is based on the energy carried by the impinging droplets being released at the surface of the liquid. As stated in Section 1 this is unlikely to occur in reality. We will now modify the model so that the energy carried by the droplets is released within the film. This adjustment is made mathematically by adding two source terms, one that depends on the droplet temperature and one on the kinetic energy. The corresponding terms are removed from the boundary conditions. The modified heat equation becomes

$$\epsilon_w\frac{\partial\theta}{\partial t} = \frac{\partial^2\theta}{\partial x^2} - \frac{\dot{m}c_wL}{hk_w}\theta + \frac{\dot{m}w^2L}{2\Delta Tk_wh}, \quad b \leqslant x \leqslant (b + h). \tag{33}$$

Note the sign change when non-dimensionalising the temperature difference $(T_a - \theta)$. Again, it is assumed that ϵ_w can be neglected leaving the leading order asymptotic form of (33)

$$\frac{\partial^2\theta}{\partial x^2} - \phi^2\theta + \gamma = 0, \quad b \leqslant x \leqslant b + h, \tag{34}$$

where $\phi = \sqrt{(\dot{m}c_wL)/(k_wh)}$ and $\gamma = (\dot{m}w^2L)/(2\Delta Tk_wh)$. This is a standard linear, constant coefficients equation, with a constant forcing term and therefore has solutions of the form $e^{\phi x}$.

Boundary condition (9) is modified so that the net heat transfer coefficient is given by

$$q_M = \lambda_e e_0 + H_{aw}.$$

The heating term becomes

$$Q_w = \frac{rH_{aw}w^2}{2c_a}.$$

The temperature in the water layer is given by

$$\theta = \frac{\gamma}{\phi^2} + \frac{e^{\phi(x-b-h)}[c_8\gamma - c_7\phi^2 + e^{-\phi h}(c_8 - \phi)(\phi^2 - \gamma)]}{\phi^2[c_8(e^{-2\phi h} - 1) - \phi(e^{-2\phi h} + 1)]} + \frac{e^{-\phi(x-b+h)}(c_7\phi^2 - c_8\gamma) + e^{-\phi(x-b)}(c_8 + \phi)(\phi^2 - \gamma)}{\phi^2[c_8(e^{-2\phi h} - 1) - \phi(e^{-2\phi h} + 1)]}. \tag{35}$$

The only remaining feature to modify is the Stefan condition, to determine the new growth rates. Differentiating Eq. (35) with respect to x and evaluating at the ice/water interface gives

$$\left.\frac{\partial\theta}{\partial x}\right|_{x=b} = \frac{(\phi^2 - \gamma)[e^{-2\phi h}(c_8 - \phi) + (c_8 + \phi)]}{\phi(c_8(e^{-2\phi h} - 1) - \phi(e^{-2\phi h} + 1))}. \tag{36}$$

Again, the height is eliminated from the Stefan condition via (30). This leaves the single equation to be solved for the ice height as

$$S\frac{\partial b}{\partial t} = d_3 - \frac{k_w}{k_i}\left.\frac{\partial\theta}{\partial x}\right|_{x=b}, \tag{37}$$

where $\partial\theta/\partial x$ is now a function of b, t only. This non-linear ODE must be solved numerically.

For both cases, with droplet energy as a boundary condition or source term, the problem has been reduced to solving a single ODE for the ice height. Once b is known then the water height may be calculated and consequently the temperature profiles. Although the analytical expressions are cumbersome this is still significantly simpler than solving the full numerical problem. In the following section we will detail the numerical scheme for the full problem and then compare results to validate the analytical expressions.

4. Numerical solution

In Section 4 an asymptotic solution was derived by neglecting the time dependence in the substrate, ice and water layers. This section is devoted to validating this assumption. Linear temperature profiles were obtained that depended only on the ice and water layer heights. The asymptotic approximation is a simplification, but to be useful must accurately approximate the solutions to the full heat Eqs. (1)–(3). The numerical model that has been developed, handles both the rime and glaze ice cases. A similar calculation has been performed by Gupta [14], using simpler boundary conditions and an iterative approach to determine the location of the solid/liquid interface.

An semi-implicit finite difference scheme was developed using standard methods found in Thomas' work [15]. A stationary grid was used for the substrate since its thickness is constant. A moving grid was used for the time dependent ice and water layers, derived from classic Stefan problems, such as in [16,17].

The same substitutions were used to non-dimensionalise all equations as in Section 3, but terms involving ϵ were not neglected.

4.1. Substrate equations

Inside the substrate, Eq. (13) may be integrated on a cell of width Δx_{sub}. Using a fully implicit scheme, this may be written as

$$\frac{\Delta t}{\epsilon_s \Delta x_{\text{sub}}^2}\chi_{i+1}^{k+1} - \left(1 + \frac{2\Delta t}{\epsilon_s \Delta x_{\text{sub}}^2}\right)\chi_i^{k+1} + \frac{\Delta t}{\epsilon_s \Delta x_{\text{sub}}^2}\chi_{i-1}^{k+1} = -\chi_i^k. \tag{38}$$

The boundary condition underneath the substrate, at $x = -1$, is determined in a similar fashion:

$$\frac{2\Delta t}{\epsilon_s \Delta x_{\text{sub}}^2}\chi_1^{k+1} - \left(1 + \frac{2\Delta t}{\epsilon_s \Delta x_{\text{sub}}^2} + \frac{2\Delta t}{\epsilon_s \Delta x_{\text{sub}}}c_1\right)\chi_0^{k+1} = -\chi_0^k + \frac{2\Delta t}{\epsilon_s \Delta x_{\text{sub}}}c_2. \tag{39}$$

The boundary condition at the top of the substrate in contact with ice at $x = 0$ becomes

$$\frac{2\Delta t}{\epsilon_s \Delta x_{\text{sub}}}c_3 T_0^{k+1} - \left(1 + \frac{2\Delta t}{\epsilon_s \Delta x_{\text{sub}}^2} + \frac{2\Delta t}{\epsilon_s \Delta x_{\text{sub}}}c_3\right)\chi_{n_{\text{sub}}}^{k+1} + \frac{2\Delta t}{\epsilon_s \Delta x_{\text{sub}}^2}\chi_{n_{\text{sub}}-1}^{k+1} = -\chi_n^k. \tag{40}$$

Eq. (40) contains T_0, which is the temperature of the ice layer at $x = 0$, hence the substrate equation is coupled to the ice equation.

4.2. Rime ice growth

The temperature profile in the ice is calculated on a moving grid with a constant number of equally spaced points. Since the height of the ice layer varies with time, the size of the mesh cell is recalculated at each time step. To account for this effect, a convection term is added to Eq. (14). The time derivative is then replaced by the total derivative. The governing equation, for example in the ice layer, becomes

$$\frac{DT}{Dt} = \frac{\partial T}{\partial t} + \frac{\partial T}{\partial x}\frac{\partial x_{\text{ice}}}{\partial t} = \frac{1}{\epsilon_i}\frac{\partial^2 T}{\partial x^2} + \frac{\partial T}{\partial x}\frac{\partial x_{\text{ice}}}{\partial t}. \tag{41}$$

where $\partial x_{\text{ice}}/\partial t$ is the speed of the moving grid.

For rime ice, all of the incoming water droplets are assumed to solidify. The ice growth rate is simply

$$\frac{\partial b}{\partial t} = 1 \text{ or } b^{k+1} = b^k + \Delta t. \tag{42}$$

The points within the ice layer are numbered from 0 at the interface with the substrate and n at the interface with the air. The two parameters $\partial x_{\text{ice}}/\partial t$ and $\Delta x_{\text{ice}}^{k+1}$ may then be evaluated as

$$\left.\frac{\partial x_{\text{ice}}}{\partial t}\right|_{i+1/2} = \frac{i+1/2}{n_{\text{ice}}}\frac{\partial b}{\partial t} = \frac{i+1/2}{n_{\text{ice}}}, \quad \Delta x_{\text{ice}}^{k+1} = \frac{b^{k+1}}{n_{\text{ice}}}.$$

The numerical scheme inside the ice layer is then

$$\left(\frac{\Delta t}{\epsilon_i \Delta x_{\text{ice}}^2} + \frac{\Delta t}{2\Delta x_{\text{ice}}}\left.\frac{\partial x_{\text{ice}}}{\partial t}\right|_{i+1/2}\right)T_{i+1}^{k+1} - \left[1 + \frac{2\Delta t}{\epsilon_i \Delta x_{\text{ice}}^2} + \frac{\Delta t}{2\Delta x_{\text{ice}}}\left(\left.\frac{\partial x_{\text{ice}}}{\partial t}\right|_{i+1/2} - \left.\frac{\partial x_{\text{ice}}}{\partial t}\right|_{i-1/2}\right)\right]T_i^{k+1} + \left(\frac{\Delta t}{\epsilon_i \Delta x_{\text{ice}}^2} - \frac{\Delta t}{2\Delta x_{\text{ice}}}\left.\frac{\partial x_{\text{ice}}}{\partial t}\right|_{i-1/2}\right)T_{i-1}^{k+1} = -T_i^k. \tag{43}$$

At the substrate/ice interface, boundary condition (20) at $x = 0$, can be approximated by

$$T_1^{k+1}\left(\frac{2\Delta t}{\epsilon_i \Delta x_{\text{ice}}^2} + \frac{\Delta t}{2\Delta x}\left.\frac{\partial x_{\text{ice}}}{\partial t}\right|_{1/2}\right) - T_0^{k+1}\left(1 + \frac{2\Delta t}{\epsilon_i \Delta x_{\text{ice}}^2} + \frac{2\Delta t c_4}{\epsilon_i \Delta x_{\text{ice}}} + \frac{\Delta t}{2\Delta x_{\text{ice}}}\left.\frac{\partial x_{\text{ice}}}{\partial t}\right|_{1/2}\right) + \chi_{n_{\text{sub}}}^{k+1}\frac{2\Delta t c_4}{\epsilon_i \Delta x_{\text{ice}}} = -T_0^k. \tag{44}$$

In this case, $\chi_{n_{\text{sub}}}$ is the temperature at the surface of the substrate. The equations for the substrate and ice layer are combined in the same matrix to ensure the algorithm is fully implicit.

At the surface of the ice layer, $x = b$, boundary condition (20) becomes

$$-T_{n_{\text{ice}}}^{k+1}\left[1 + \frac{2\Delta t}{\epsilon_i \Delta x_{\text{ice}}^2} + \frac{2\Delta t c_6}{\epsilon_i \Delta x_{\text{ice}}} - \frac{\Delta t}{2\Delta x_{\text{ice}}}\left.\frac{\partial x_{\text{ice}}}{\partial t}\right|_{n_{\text{ice}}-1/2} + \frac{c_6 \Delta t}{2}\left.\frac{\partial x_{\text{ice}}}{\partial t}\right|_{n_{\text{ice}}}\right] + T_{n_{\text{ice}}-1}^{k+1}\left(\frac{2\Delta t}{\epsilon_i \Delta x_{\text{ice}}^2} - \frac{\Delta t}{2\Delta x}\left.\frac{\partial x_{\text{ice}}}{\partial t}\right|_{n_{\text{ice}}-1/2}\right) = -T_{n_{\text{ice}}}^k - \frac{2\Delta t c_5}{\epsilon_i \Delta x_{\text{ice}}} - \frac{c_5 \Delta t}{2}\left.\frac{\partial x_{\text{ice}}}{\partial t}\right|_{n_{\text{ice}}}. \tag{45}$$

Solving for the temperature in the substrate and the rime ice layer reduces then to inverting a single tri-diagonal matrix. The numerical solution in the substrate and ice is given by constructing a tri-diagonal matrix using the order $(\chi_0 .. \chi_{n_{\text{sub}}}, T_0 .. T_{n_{\text{ice}}})$. The substrate equations are given by (38)–(40) and the ice layer equations are given by (43)–(45). The terms in the ice equations need to be updated at each time step as the mesh is changing. Inverting this

matrix completely solves the system for temperature in the ice and substrate.

4.3. Glaze ice growth

The rime model is run until the surface temperature exceeds unity ($T = T_f = 1$). Once $T(b) \geqslant 1$, the surface ice temperature is truncated to unity and the calculation for the water layer is activated.

At the top of the ice layer, heat flux boundary condition (20) is changed to (21)a. This requires ensuring

$$T_{n_{ice}} = 1 \quad \text{and} \quad \theta_0 = 1. \tag{46}$$

The ice and water layer thicknesses are linked through the speed of the growth rates, determined by the temperature gradients at $x = b$, using the Stefan condition (18):

$$\frac{\partial b}{\partial t} = S^{-1}\left(\frac{\partial T}{\partial x} - \frac{k_w}{k_i}\frac{\partial \theta}{\partial x}\right) = S^{-1}\left(\frac{3 - 4T^k_{n_{ice}-1} + T^k_{n_{ice}-2}}{2\Delta x_{ice}} - \frac{k_w}{k_i}\frac{\left(-3 + 4\theta^k_1 - \theta^k_2\right)}{2\Delta x_{wat}}\right). \tag{47}$$

The change of the water layer height is then given by mass conservation (17)

$$\frac{\partial h}{\partial t} = \frac{\rho_i}{\rho_w}\left(1 - \frac{\partial b}{\partial t}\right). \tag{48}$$

Since the water layer height is zero at $t = t_w$, it is necessary to either define a thin precursor water layer, or set the temperature gradient of the water layer in (47) to be very small. Either approach produces the same results, but is required to start the solution, for the first time step only.

The ice and water layer thicknesses can then be determined by

$$b^{k+1} = b^k + \frac{\partial b}{\partial t}\Delta t, \quad h^{k+1} = h^k + \frac{\partial h}{\partial t}\Delta t. \tag{49}$$

The grid spacing and the two parameters $\partial x_{ice}/\partial t$ and $\partial x_{wat}/\partial t$ must be recalculated for each layer at every time step,

$$\text{Ice:} \quad \Delta x^{k+1}_{ice} = \frac{b^{k+1}}{n_{ice}}, \quad \left.\frac{\partial x_{ice}}{\partial t}\right|_{i+1/2} = \frac{i + 1/2}{n_{ice}}\frac{\partial b}{\partial t},$$

$$\text{Water:} \quad \Delta x^{k+1}_{wat} = \frac{h^{k+1}}{n_{wat}}, \quad \left.\frac{\partial x_{wat}}{\partial t}\right|_{i+1/2} = \frac{i + 1/2}{n_{wat}}\frac{\partial h}{\partial t}.$$

The numerical schemes developed in the previous sections inside the substrate and the ice layer remain valid. The boundary condition at the top of the ice surface (45) only is modified and replaced by the condition $T_{n_{ice}} = 1$. Inside the water layer, the numerical scheme is derived similarly as for the ice layer:

$$\left(\frac{\Delta t}{\epsilon_w \Delta x^2_{wat}} + \frac{\Delta t}{2\Delta x_{wat}}\left.\frac{\partial x_{wat}}{\partial t}\right|_{i+1/2}\right)\theta^{k+1}_{i+1} - \left[1 + \frac{2\Delta t}{\epsilon_w \Delta x^2_{wat}} + \frac{\Delta t}{2\Delta x_{wat}}\left(\left.\frac{\partial x_{wat}}{\partial t}\right|_{i+1/2} - \left.\frac{\partial x_{wat}}{\partial t}\right|_{i-1/2}\right)\right]\theta^{k+1}_i + \left(\frac{\Delta t}{\epsilon_w \Delta x^2_{wat}} - \frac{\Delta t}{2\Delta x_{wat}}\left.\frac{\partial x_{wat}}{\partial t}\right|_{i-1/2}\right)\theta^{k+1}_{i-1} = -\theta^k_i. \tag{50}$$

At the top of the water layer, the flux boundary condition (21) is given by

$$-\theta^{k+1}_{n_{wat}}\left[1 + \frac{2\Delta t}{\epsilon_w \Delta x^2_{wat}} + \frac{2\Delta t c_8}{\epsilon_w \Delta x_{wat}} - \frac{\Delta t}{2\Delta x_{wat}}\left.\frac{\partial x_{wat}}{\partial t}\right|_{n_{wat}-1/2} + \frac{c_8 \Delta t}{2}\left.\frac{\partial x_{wat}}{\partial t}\right|_{n_{wat}}\right] + \theta^{k+1}_{n_{wat}-1}\left(\frac{2\Delta t}{\epsilon_w \Delta x^2_{wat}} - \frac{\Delta t}{2\Delta x}\left.\frac{\partial x_{wat}}{\partial t}\right|_{n_{wat}-1/2}\right) = -\theta^k_{n_{wat}} - \frac{2\Delta t c_7}{\epsilon_w \Delta x_{wat}} - \frac{c_7 \Delta t}{2}\left.\frac{\partial x_{wat}}{\partial t}\right|_{n_{wat}}. \tag{51}$$

Since the water layer temperatures are not directly coupled to the ice layer, these equations can be solved in a separate matrix. Solving the glaze ice case consists of constructing and solving two systems of equations and is summarised in Fig. 4. One matrix is required for the ice and substrate with the constant temperature boundary condition (46); and another matrix is required for the water layer using Eqs. (50) and (51). Inverting these matrices will give the complete temperature profile of the glaze ice system for the current time step.

After Δt the ice and water growth rates are recalculated using (47) and (48) with the recent temperature profile. The next ice and water layer heights are then given by Eq. (49), which can be used to formulate the substrate/ice and water matrices. This may be repeated for the time interval of interest.

5. Results

The most interesting results (and challenging to compute) occur under glaze ice conditions, since we first see rime ice and then a transition to glaze. From Fig. 2 we can see the range of temperatures where glaze ice will occur. In the subsequent calculations we take $T_A = T_a = 271.1$ K and $T_A = T_a = 260.0$ K for structural and aircraft conditions respectively. These temperatures are at the high end of the scale and should lead to a relatively thick water layer.

5.1. Validation of the asymptotic model

For comparison purposes both the numerical and asymptotic models were solved until $t = 4$, which is approximately $2t_w$. Fig. 5 shows the height profile and temperature of glaze on a substrate under structural icing conditions (when the droplet thermal energy is included as a boundary condition).

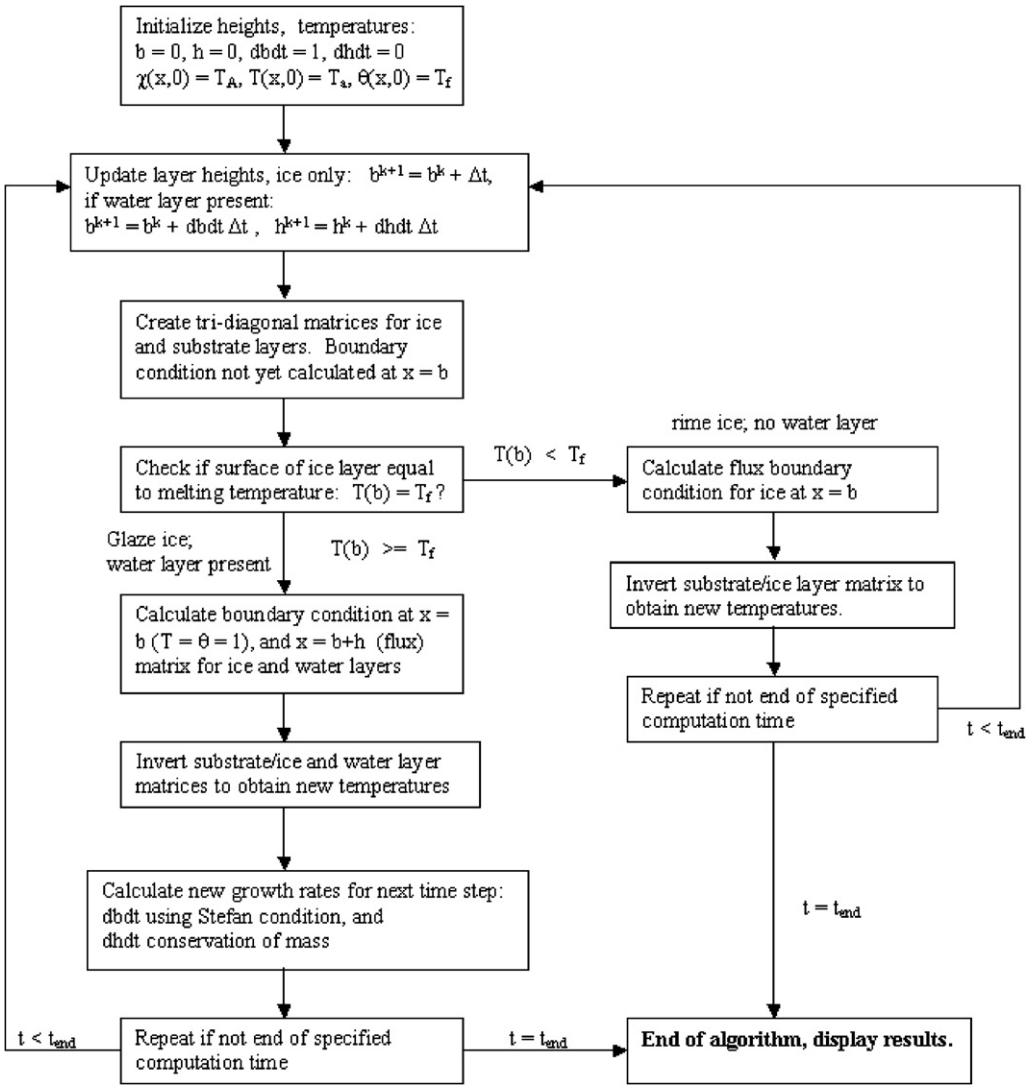

Fig. 4. Summary of algorithm used in numerical solution.

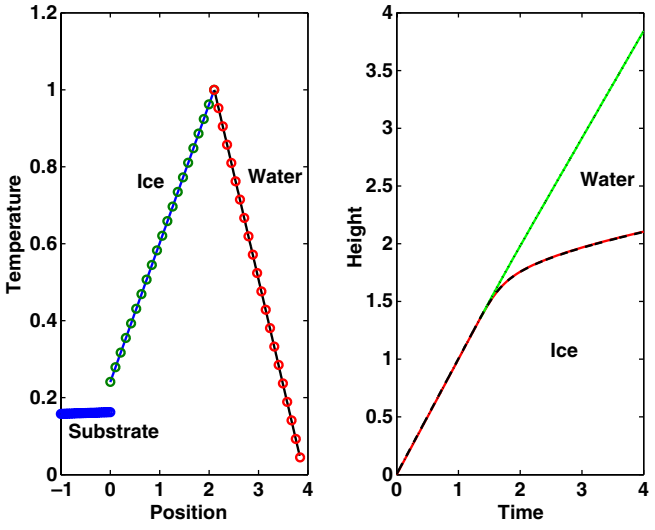

Fig. 5. Temperature profile at time $t = 4$ (right) and height profile for $t \in [0,4]$ (left) for glaze ice formation under structural icing conditions.

A total of 20 mesh points were used in the numerical solution with 1000 time steps. The solid lines are the asymptotic results and the circles/dotted lines are the numerical values. For both temperature and height the asymptotic profiles agree to within 1% of the numerical values. This indicates that the asymptotic model is valid for all time.

Fig. 6 shows corresponding results for calculations carried out under aircraft icing conditions. Again good agreement is shown between the asymptotic and numerical solutions.

The time at which water forms, t_w, was also compared (this is where the graphs for height split). This is believed to be a good comparison because it comprises the time dependence and the heat distribution. The values for t_w were within 3% for the aircraft case and 2% for the structural case.

Doubling the number of grid points or time steps in the numerical solution did not change the results significantly. Specifically, the time to water appearing varied by less than 0.1%.

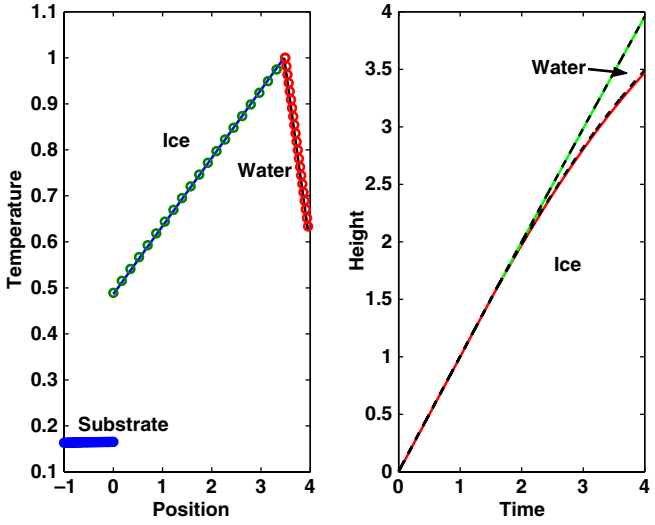

Fig. 6. Temperature profile at time $t = 4$ (right) and height profile for $t \in [0,4]$ (left) for glaze ice formation under aircraft icing conditions.

5.2. The effect of droplet energy

We now compare results where the droplet energy is included in the boundary condition or as a source term. In the previous subsection, the asymptotic and numerical solutions were shown to be almost identical when the droplet energy is applied at the boundary. Our numerical studies have shown the same to be true when it is included as a source term. The contrast of interest is therefore between the different models themselves. The two asymptotic models are compared in Fig. 7 for typical structural icing conditions, the source term model is plotted with solid lines and the boundary condition model is in dotted lines/circles. Clearly the temperature predictions are almost identical throughout the calculation. The main difference being that the ice height is slightly greater for the source term model.

In Fig. 8 the equivalent curves are shown under aircraft icing conditions. In this case significant differences can be

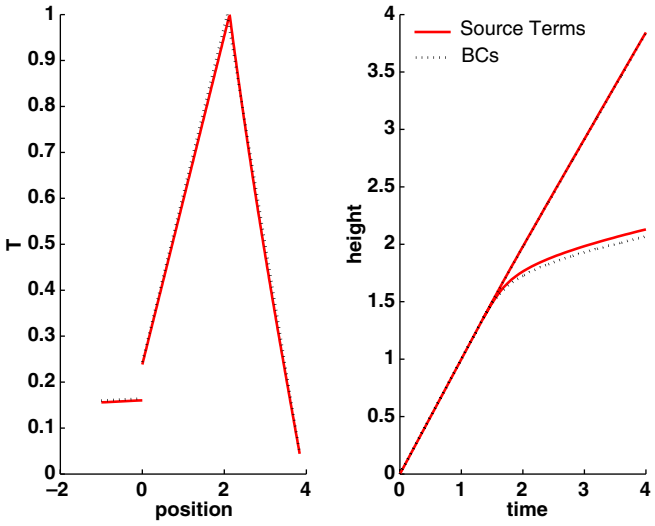

Fig. 7. Comparison of droplet energy models for structural icing.

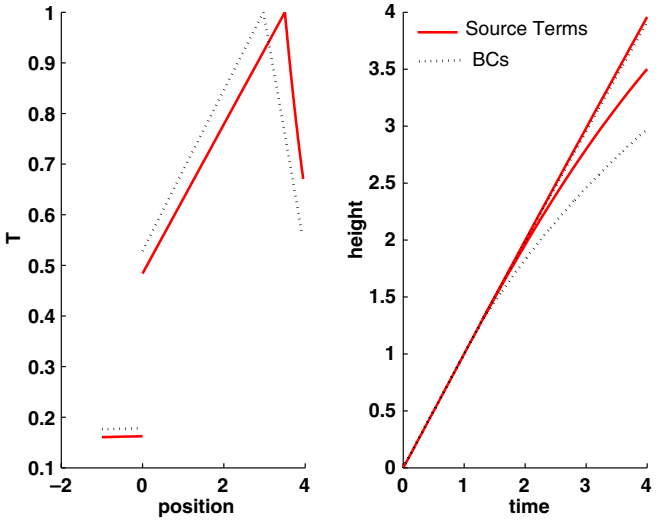

Fig. 8. Comparison of droplet energy models for aircraft icing.

observed. With the source term model the temperature in the substrate and ice is lower than with the boundary condition model. Consequently, the ice layer is significantly thicker and water appears after a much longer time.

The obvious conclusion is then, at least for aircraft icing conditions, that a source term model is the safest to apply since the boundary condition model may underpredict the ice thickness. For structural icing the difference is not so crucial. Either model can therefore be safely used in this case. Of course these conclusions are only valid for the cases investigated during this study. In fact the two terms that have been used as energy sources in the heat equation have competing effects. Currently the cooling by the droplets appears to dominate and so acts to decrease the water layer temperature. However, it is possible that, if all other terms are held constant, and the far field velocity increased then the kinetic energy would increase sufficiently to dominate over the droplet cooling and heat up the water, so decreasing the ice layer thickness. But this scenario is really only likely for aircraft icing.

6. Conclusions

The main objectives of this study were:

(a) To determine an asymptotic model for ice accretion on a conducting substrate.
(b) To determine whether the asymptotic model in this and previous studies is valid for small times.
(c) To determine whether applying the droplet energy into the water layer has a significant effect on the accretion model.

The asymptotic model, though algebraically awkward, was successfully developed. Comparison of the asymptotic and numerical models showed excellent agreement. The obvious inference is that the asymptotic model in the

present work and in previous simpler models, [6,5], are valid for all time, despite the relatively large values of ϵ_w.

The question concerning droplet energy is more complicated. Firstly, there are two competing effects: the droplet kinetic energy increases the film temperature whereas the droplet temperature reduces it. Under aircraft icing conditions the droplets are very fast moving and so the kinetic energy makes a significant contribution to the energy balance. However, the rate at which droplets impact is also high so their temperature also contributes significantly. In the simulations shown the result is that the ice grows more rapidly if the energy is applied within the film. For structural icing the low velocities and rate at which mass accumulates leads to little difference between the two models. Consequently it appears that for structural icing there is little to choose between the models. However, in general it must be best to apply the energy term throughout the film since this is probably the most realistic scenario and, under certain conditions, it can lead to significantly increased ice growth rates. Clearly, for safety reasons, it is important to predict the upper limit for any accretion.

Acknowledgements

T.M. acknowledges the support of this work by the National Research Foundation of South Africa, under grant number 2053289 as well as the Korean Advanced Institute of Science and Technology. J.C. acknowledges the financial support of the Claude Leon Foundation.

References

[1] R.W. Gent, N.P. Dart, J.T. Cansdale, Aircraft icing, Philos. Trans. R. Soc. London, A 358 (1776) (2000) 2873–2911.
[2] E.P. Lozowski, K. Szilder, L. Makkonen, Computer simulation of marine ice accretion, Philos. Trans. R. Soc. London, A (358) (2000) 2811–2845.
[3] G.I. Poots, Ice and Snow Accretion on Structures, Research Studies Press, 1996.
[4] B.L. Messinger, Equilibrium temperature of an unheated icing surface as a function of air speed, J. Aero. Sci. (January) (1953) 29–42.
[5] T.G. Myers, An extension to the Messinger model for aircraft icing, AIAA J. 39 (2) (2001) 211–218.
[6] T.G. Myers, D.W. Hammond, Ice and water film growth from incoming supercooled droplets, Int. J. Heat Mass Transfer 42 (1999) 2233–2242.
[7] T.G. Myers, J.P.F. Charpin, C.P. Thompson, Slowly accreting glaze ice due to supercooled water impacting on a cold surface, Phys. Fluids 14 (1) (2002) 240–256.
[8] T.G. Myers, J.P.F. Charpin, S.J. Chapman, The flow and solidification of a thin fluid film on an arbitrary three-dimensional surface, Phys. Fluids 14 (8) (2002) 2788–2803.
[9] P. Bartlett, Development of a new model of ice accretion on aircraft, in: Proceedings of 9th International Workshop on Atmospheric Icing on Structures, Chester, UK, June 2000.
[10] G.F. Naterer, Coupled liquid film and solidified layer growth with impinging supercooled droplets and Joule heating, Int. J. Heat Fluid Flow 24 (2003) 223–235.
[11] T.G. Myers, J.P.F. Charpin, A mathematical model for atmospheric ice accretion and water flow on a cold surface, Int. J. Heat Mass Transfer 47 (2004) 5483–5500.
[12] A.C. Fowler, Mathematical Models in the Applied Sciences, Cambridge University Press, 1998.
[13] E.J. Hinch, Perturbation Methods, Cambridge University Press, 1994.
[14] S.C. Gupta, E. Laitinen, T. Valterri, Moving grid scheme for multiple moving boundaries, Comput. Methods Appl. Mech. Eng. 167 (1998) 345–353.
[15] J.W. Thomas, Numerical partial differential equations – finite difference methods, Texts in Applied Mathematics, vol. 22, Springer, 1995.
[16] Rizwan-Uddin, A nodal method for phase change moving boundary problems, Int. J. Comput. Fluid Dyn. 11 (1999) 211–221.
[17] S. Kutluay, A.R. Bahadir, A. Ozde, The numerical solution of one-phase classical Stefan problem, J. Comput. Appl. Math. 81 (1997) 35–144.